CHAPTER 4

RESULTS AND DISCUSSION

4.1 Introduction

This chapter explains, describes, and highlights this study's experiments. This chapter also presents results and discusses observations using the CCD tomography system for grading and determining the valuation of the clarity of the ruby stones, with the help of the CCD linear sensors and the LabVIEW program.

The results presented in this chapter focused on the following points:

i. Analyzing the ability of the CCD tomography system to differentiate between different refractive indices of ruby stones via a simulation model.

ii. Analyzing the CCD tomography system's performance when grading ruby stones with and without a laser as a transmitter via a simulation model.

iii. Analyzing the CCD tomography system's ability to validate the optical properties of ruby stones via data from the simulation and experimental.

The research used Minitab 16 software for statistical calculations and analysis. In this study, the researchers used the t-test to validate the no. of pixels in the reconstructed image to compare the targeted (population) mean value with the experiment sample mean value shown in the third analysis in this chapter.

The two-sample t-test is for cases of unknown variance to determine whether an unknown population mean is different from a specific value, and the samples are independent (Glen, 2022; Jamaludin, 2016; Stuart & Ross, 1988).

The Z-axis represents the pixel values based on the reconstructed images of the rubies.

This method was chosen to evaluate the optical properties of ruby stone clarity due to existing studies. These extant studies showed that the CCD tomography system was the best tool for analyzing the Z-axis as it could differentiate between the different transparencies of the measured objects (Jamaludin, 2013b, 2016; Jamaludin et al., 2014, 2015, 2020; Jamaludin, Abdul Rahim, et al., 2016; Jamaludin, Rahim, Rahim, et al., 2017; Jamaludin & Abdul Rahim, 2016).

4.2 Analysing the Ability of the CCD Tomography System to Differentiate between Different Refractive Index Values

This study obtained simulation results by running an algorithm in LabVIEW. This simulation was conducted to review the characteristics of light as it travels through a ruby stone to a CCD sensor. The light intensity was the controller, while the results of the LabVIEW simulation were the indicator. Statistical analysis was also conducted to determine the ability of the CCD tomography system to distinguish between different types of image reconstruction systems with different RI values of ruby stones.

Here, the research discusses and compares two different image reconstruction systems developed using the ruby stones' lowest and highest RI values. The highest RI value of ruby stone was 1.770, while the lowest RI value was 1.762 (Fuller et al., 2014). As mentioned in the research methodology, two types of image reconstruction systems were discussed;

i. Image reconstruction for System A (laser-ruby stone-CCD)
ii. Image reconstruction for System B (ruby stone-CCD)

The t-test analysis validated the CCD tomography simulation system using LabVIEW to distinguish between ruby stones based on their refractive indices. The t-test determines whether an unknown population mean differs from a specific value, and the hypotheses of this analysis were:

H_0: Mean of ruby stones with lowest refractive index = Mean of ruby stones with highest refractive index.

H_1: Mean of ruby stones with lowest refractive index ≠ Mean of ruby stones with highest refractive index.

The null hypothesis (H_0) proposed that the CCD tomography system did not detect differences when measuring the highest and lowest RI. Meanwhile, the alternative hypothesis (H_1) suggests that there is a difference.

4.2.1 Image Reconstruction for System A

The image reconstruction for System A is displayed in the block diagram in Figure 3.7. Table 4.1 provides the results, in terms of its image reconstruction based on the final light intensity ratio and voltage output of the CCD.

Table 4.1: A Comparison of Different RI Values for The Ruby Stone (System A)

Characteristic	Lowest Refractive Index	Highest Refractive Index
Refractive Index of Ruby Stone (M. Fuller, B. W. Smigel, J. I. Koivula, 2014)	1.762	1.770
Final light intensity ratio $\frac{I_{2'}}{I_i}$	0.8478	0.8455
V= -2.78I + 4.3	1.994	2.000
Three-Dimensional form	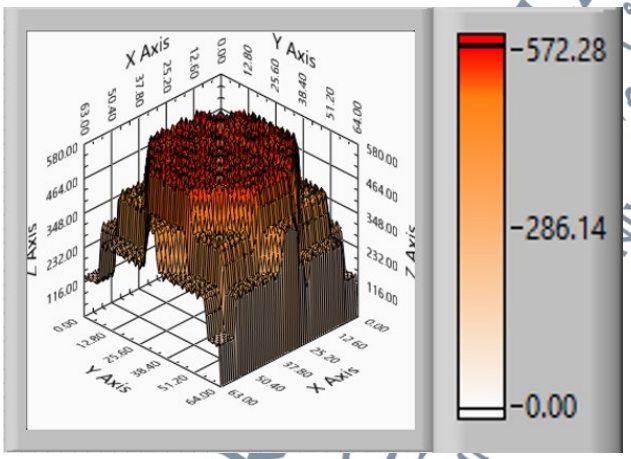 Z-axis ≤ 572.28	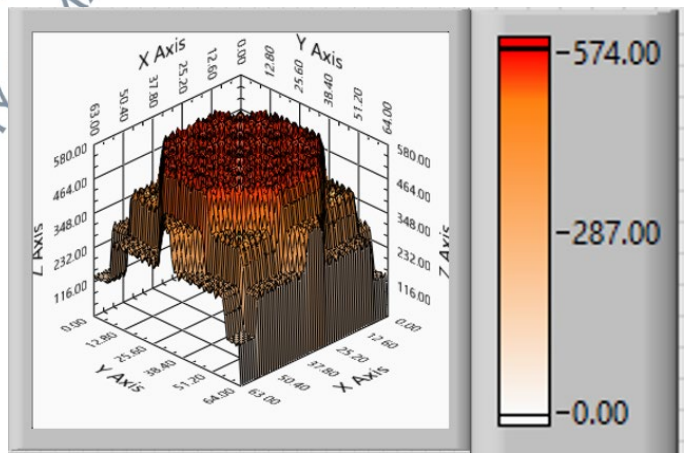 Z-axis ≥ 572.28

For the 3D images form in this chapter, there are 3 axis that will appear which are x, y and z-axes. The conceptual modeling for the grading of ruby stone is gained from the Z-axis, which represents the grading clarity of each RI depicted by the ruby stone (Jamaludin, 2016; Mohd Rahalim et al., 2021). The Z-axis value is shown by the bar graph at the right side of the picture; it represents the pixel values based on the reconstructed images of the rubies. The pixels value was varied based on the RI of the ruby stone.

4.2.2 Statistical Analysis of the Image Reconstruction for System A

The statistical analysis of the image reconstruction for system A uses the two-sample t-test since the sample data is independent to one of each other (Glen, 2022). Besides, the two-sample t-test is used to determine whether or not two population means are equal. The mean result from the effective pixels of the image for the lowest and highest RI of ruby stone are analyzed to validate the hypothesis for this simulation.

As shown in Figure 4.1, the average value of the higher RI was 515.35, while the mean low RI value was 509.09. The difference between the two mean values was 6.26. The system showed a p-value of 0, which was <0.05. Thus, the null hypothesis was rejected for the image reconstruction system, which included the laser-ruby stone-CCD. The research concluded that the CCD tomography technique could measure the differences between the two RI values.

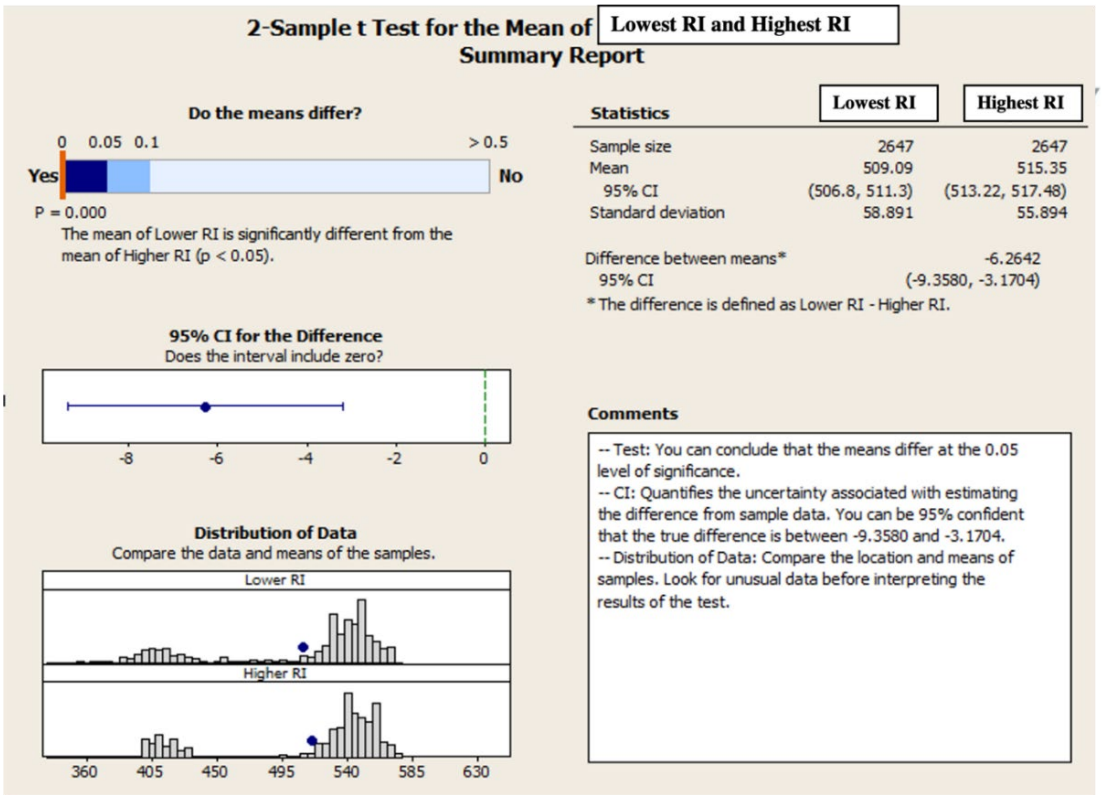

Figure 4.1: Summary of the 2-Sample T-Test for The Mean of The Lowest and Highest RI (System A)

4.2.3 Image Reconstruction for System B

The image reconstruction for System B is displayed in the block diagram in Figure 3.8. Table 4.2 provides the results, in terms of its image reconstruction based on the final light intensity ratio and voltage output of the CCD.

Table 4.2: Comparison of The Varying Ruby Stone Refractive Indices of System B

Characteristic	Lowest Refractive Index	Highest Refractive Index
Refractive Index (RI) of Ruby Stone (M. Fuller, B. W. Smigel, J. I. Koivula, 2014)	1.762	1.770
Final light intensity ration $\frac{I_{2'}}{I_i}$	0.9239	0.9227
V= -2.78I + 4.3	1.7887	1.7919
Three-Dimensional form	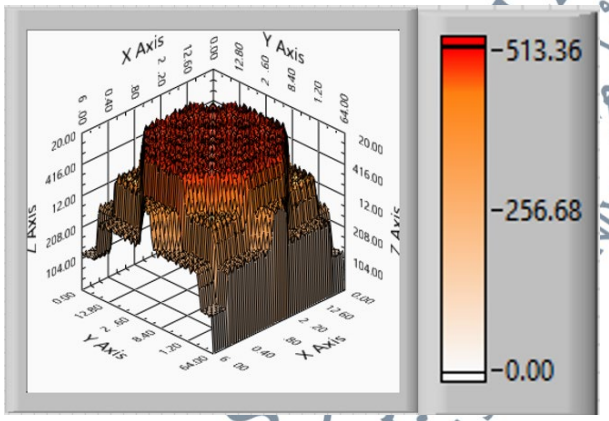 Z axis ≤ 513.36	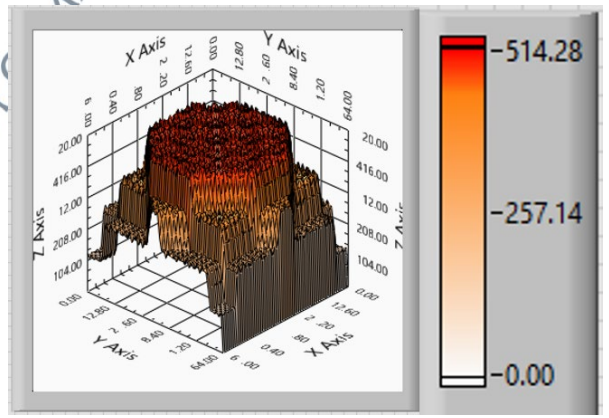 Z axis ≥513.36

4.2.4 Statistical Analysis of the Image Reconstruction for System B

The statistical analysis of the image reconstruction for system B is done with the two-sample t-test. The mean result from the effective pixels of the image for the lowest and highest RI of ruby stone are analyzed to validate the hypothesis for this simulation. Besides, the individual plot for the highest and lowest RI of ruby stone is also been visualized in Figure 4.3 to compare the difference between mean pixels value of both images reconstructed in System B.

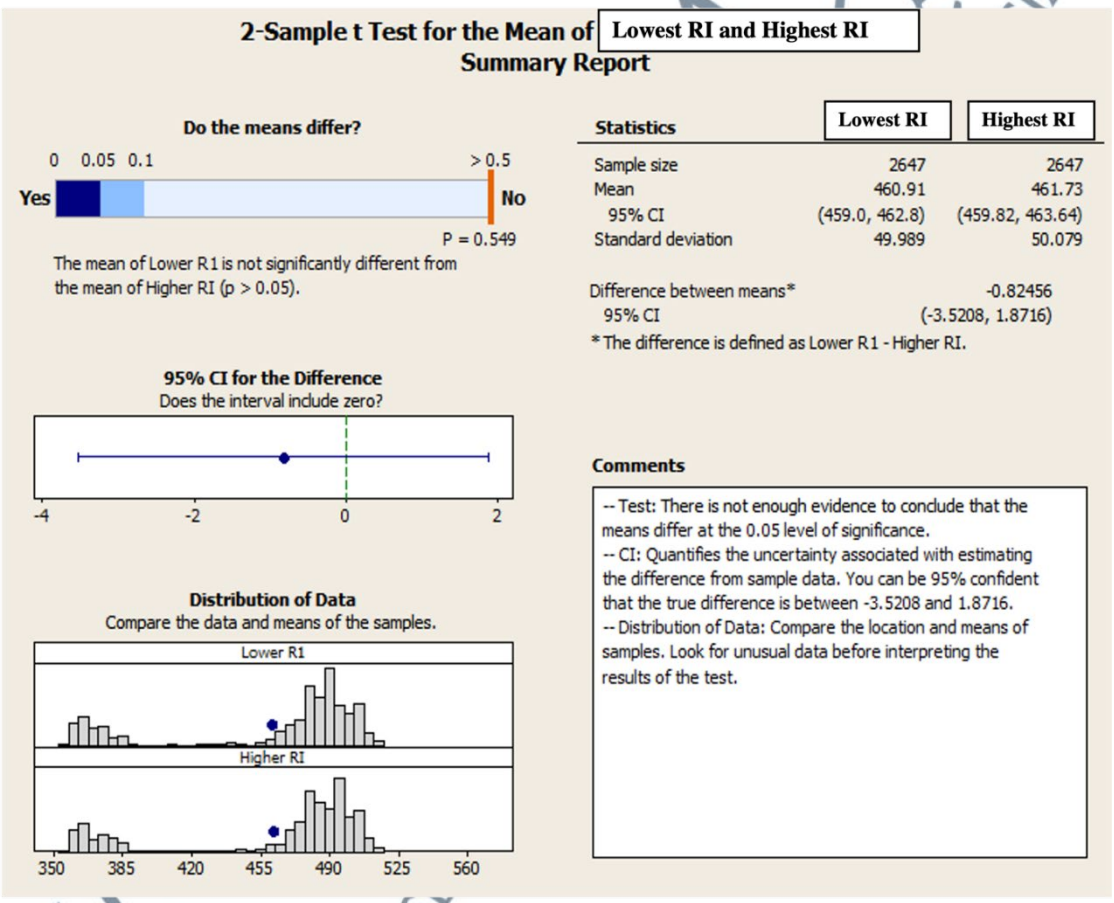

Figure 4.2: Summary of the 2-Sample T-Test for The Mean of The Lowest and Highest RI (System B)

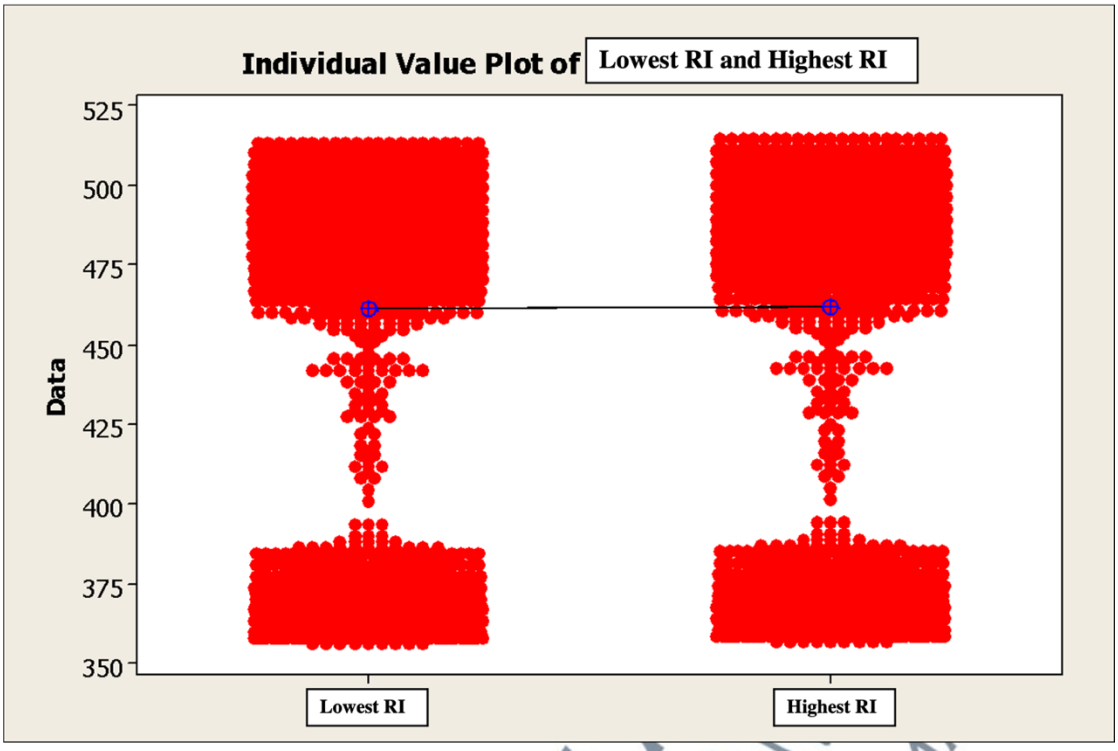

Figure 4.3: Individual Plot of Lowest and Highest RI (System B)

As seen in Figure 4.2, the mean of the higher RI was 461.73, while the mean of the Lowest RI was 460.91. This was a 0.82 difference in mean values. Based on the summary of the two-sample t-test for the mean of the lowest and highest RI (System B), the p-value was greater than zero. This meant that the null hypothesis for this image reconstruction system, which consisted of a ruby stone-CCD, was accepted. The null hypothesis posited that the mean voltage output of the lowest RI was equal to that of the highest RI. However, as seen in Figure 4.3, the mean voltages of the lower and higher RIs did not differ. Instead, there was an overlap between the mean voltage outputs, within 450 to 475 pixels. The research concluded that the CCD tomography technique could not measure the differences between the two differing values of the RI in the system without the help of a laser transmitter.

4.3 Analysing the Performance of the CCD Tomography System in Grading Ruby Stone

In this study, the research analyzed two types of image reconstruction systems. The 1st is the CCD tomography system consisting of a laser transmitter (System A), while the 2nd system is the CCD tomography system without the laser transmitter (System B). Light transmitted to the CCD is analyzed to determine the final light intensity. Lastly, the research determined the simulation image output and used statistical analysis for analyzing and comparing the ability of the two CCD tomography image reconstruction systems.

4.3.1 Image Reconstruction for System A

Figure 3.7 depicts the image reconstruction for System A while Table 4.3 provides its image reconstruction according to the final light intensity ratio and voltage output of the CCD.

4.3.2 Image Reconstruction for System B

Figure 3.8 depicts the image reconstruction for System B while Table 4.4 provides its image reconstruction according to the final light intensity ratio and voltage output of the CCD.

Table 4.3: Comparison for The Varying Ruby Stone Refractive Indices of System A

Characteristic	Lowest Refractive Index	Highest Refractive Index
Refractive Index of Ruby Stone (M. Fuller, B. W. Smigel, J. I. Koivula, 2014)	1.762	1.770
Three-Dimensional form	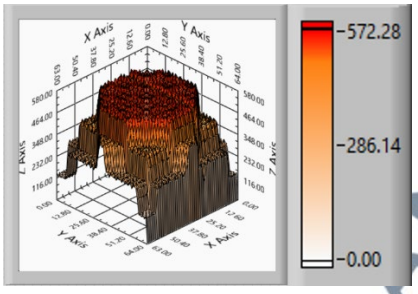 Z-axis ≤ 572.28	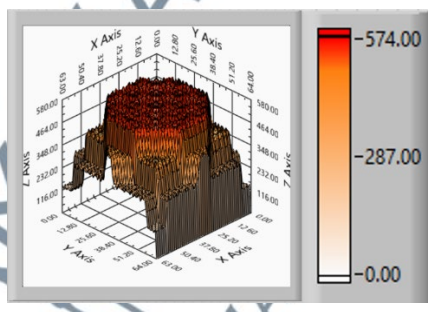 Z-axis ≥ 572.28

Table 4.4: Comparison for The Varying Ruby Stone Refractive Indices of System B

Characteristic	Lowest Refractive Index	Highest Refractive Index
Refractive Index (RI) of Ruby Stone (M. Fuller, B. W. Smigel, J. I. Koivula, 2014)	1.762	1.770
Three-Dimensional form	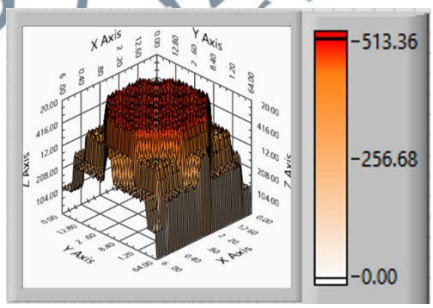 Z-axis ≤ 513.36	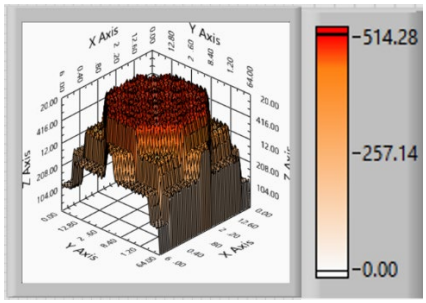 Z-axis ≥ 513.36

4.3.3 Differences between the Image Outputs of the CCD Tomography System

Sections 4.2.1 and 4.2.3 provide the image outputs of simulations run with two different refractive indices for the ruby stones. Section 4.2.1 provides the image reconstruction for System A, the laser-ruby stone-CCD, while Section 4.2.3 provides the image reconstruction for System B, the ruby stone-laser. The research used the mathematical algorithm described in Chapter 3 and varied the final light intensity ratio of ruby stone based on the image reconstruction system and RI value of the ruby stone.

Table 4.3 and Table 4.4 present the 3D form, which included Z-axis analysis for all experiments using different RI values. The Z-axis presents the pixel values depending on the multiplication results of sensitivity maps for the 160 views using the CCD normalized voltage value (5 V) (Sony Corporation, n.d.). A different transparency level will offer a different Z-axis. A higher transparency level generates a lower Z-axis, while a higher opacity generates a higher Z-axis. The ruby transparency is represented by the clarity which depends on the refractive index of this stone. Table 4.3 and Table 4.4 present the 3D images validating that a low RI value of the ruby stone showed a low Z-axis value for both the image reconstruction systems (A and B).

The result shows that, for lowest RI value, the Z-axis value will be lower than the highest RI value of ruby stone. Therefore, we could identify the range of the natural ruby stone based on the range of the Z-axis value which clarifies the grading valuation of ruby stone based on its clarity feature (Abdul Rahim & San, 2008; Grande & Augustyn, 2010; Jamaludin, 2013a, 2016; Jamaludin et al., 2015; Jamaludin, Abdul Rahim, et al., 2016; Mohd Rahalim et al., 2021; Shaban & Tavoularis, 2017; Sony Corporation, n.d.).

Based on the observation of two reconstructions (System A and System B), the results showed a significant difference in the Z-axis between the maximal and minimal RI value ranges described in the Gemology Tools (Nassau, 2003) when the research used System A (containing the laser as a transmitter) for image reconstruction. Table 4.5 presents the comparison between the 3D images derived for Systems A and B.

Table 4.5: Comparison of the 3D Images of Both Systems

Charac-teristic	System A	System B
1.762	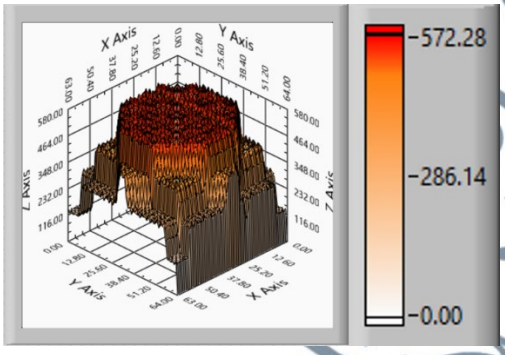 Z axis: 572.28	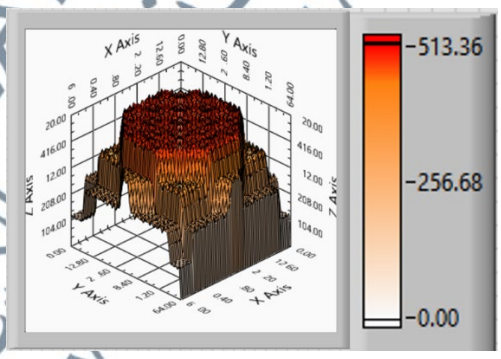 Z axis: 513.36
1.770	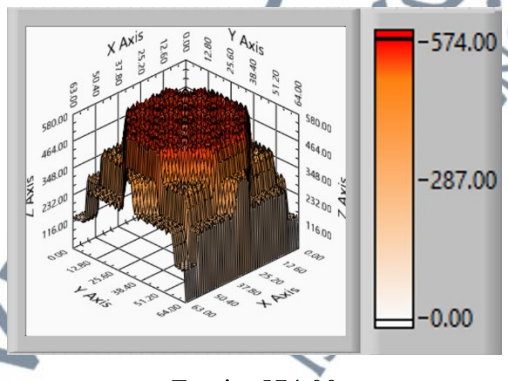 Z axis: 574.00	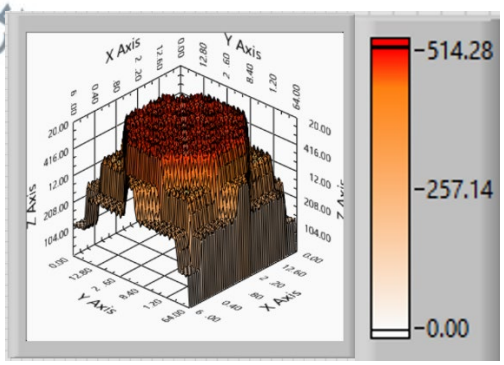 Z axis: 514.28

4.3.4 Statistical Analysis of Differences between the Image Outputs of the CCD Tomography System

The same RI value, 1.770, was selected. These values were between two different CCD tomography systems, with a laser as a transmitter and the other without, were compared. Figure **4.4** compares the two-sample t-test results of image reconstructions in Systems A and B.

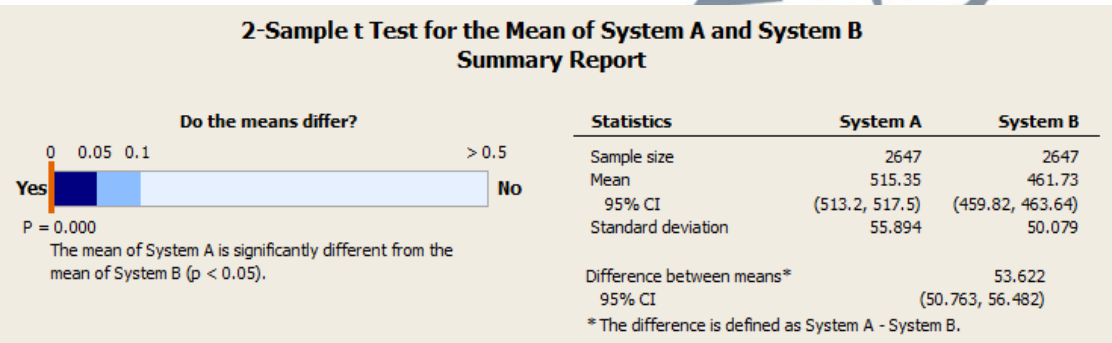

Figure 4.4: Summary of the 2-Sample T-Test for The Mean Voltage Outputs of Systems A and B

The hypotheses of this analysis were:

H_0: Mean pixel value for ruby stones in System A = Mean pixel value for ruby stones in System B.

H_1: Mean pixel value for ruby stones in System A ≠ Mean pixel value for ruby stones in System B.

The research proposed a null hypothesis, H_0, that the CCD tomography system could detect no significant difference that consisted/ did not consist of a laser while

measuring the high RI value of the ruby stone. They also proposed an alternative hypothesis, H_1, that the technique could detect the differences.

As seen in Figure 4.4, the two-sample t-test indicated the p-value was less than 0.05. Therefore, the null hypothesis was rejected and the alternative hypothesis, the mean pixel value of ruby stones in System A did not equal to the mean pixel value of ruby stones in System B, was accepted. Figure 4.5 depicts the distribution of data between Systems A and B. The mean pixel value of System A was higher than that of System B.

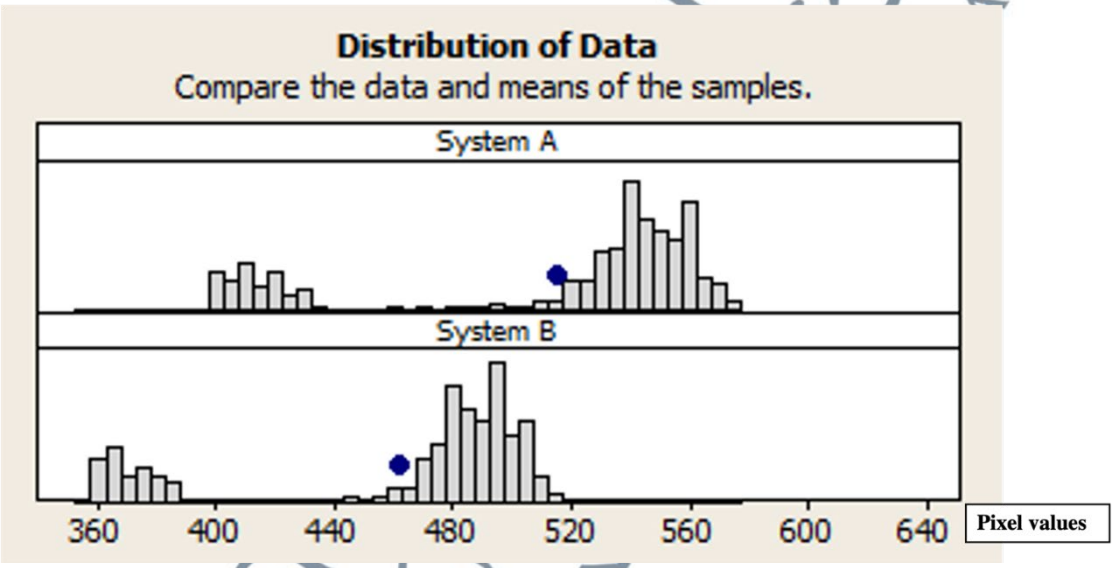

Figure 4.5: Mean Pixel Values of Systems A and B

4.3.5 Observations

The Z-axis presents the pixel values based on the multiplication results for the sensitivity maps for 160 views with CCD normalized voltage values (5 V) (Sony Corporation, n.d.). Figure 4.5 shows the voltage output of the Z-axis of System A (with a laser as a transmitter) was higher. As such, only the system with a laser as a transmitter

was considered for further analysis. Furthermore, unlike System A, the two refractive index ranges did not differ significantly when System B was applied, as shown by the differences between the mean pixel values of both refractive indices of the two image reconstruction systems. Table 4.6 provides the mean pixel values for better visualisation.

Table 4.6: Comparison of The Mean Pixel Values of The Two Refractive Indices of Ruby Stones

Type of Image Reconstruction System	System A	System B
Difference for mean of pixel values between two different refractive indices of the ruby stone	6.26	0.82

Based on this statistical analysis, only the system with the laser was considered for further real-time analysis as it could better distinguish between the two refractive indices of ruby stones.

4.4 Analysing the Ability of the CCD Tomography System to Validate the Optical Properties of Ruby Stones

This section discusses the use experiment that was conducted to evaluate the performance of the image reconstruction with a laser as a transmitter. The CCD tomography system and LabVIEW programming software were used to quantitatively grade a ruby stone.

4.4.1 CCD Voltage Output

Two CCD voltage outputs, the theoretical values of Systems A and B and their respective light intensities, were compared.

4.4.1.1 Theoretical CCD Voltage Output

Based on the initial state of the CCD tomography system, the equation showed that the voltage gained was V= −2.78I + 4.3 (Table 4.7). Therefore, based on the final light intensity ratio, the voltage was as stated in the table below.

Table 4.7: Theoretical CCD Voltage Output

Final light intensity ratio, $\frac{I_{2'}}{I_i}$	**Voltage, V**
0.8478	1.994
0.8455	2.000

4.4.1.2 Experimental CCD Voltage Output

In this study, eight samples were collected from the ruby stone at room temperature ranging between 25° and 33°C, with relative humidity ranging between 65% and 85%, using the KT-903 humidity device. The samples noted minimal light scattering and diffraction effects, which were further ignored during calculations. The samples maintained the luminosity for the lasers at 0.3 Lux. Figure 4.6 and Table 4.8 summarize the CCD tomography voltages of eight ruby stone samples and the mean voltage of each sample, respectively.

Descriptive Statistics: CCD Mean VoltageValue for Eight Samples of Ruby Stones When Laser is ON

Variable	N	N*	Mean	SE Mean	StDev	Minimum	Q1
CCD Voltage Output Value (V)_1	600	0	1.5104	0.00128	0.0314	1.4200	1.5000
CCD Voltage Output Value (V)_2	600	0	0.59354	0.00133	0.03251	0.54200	0.58300
CCD Voltage Output Value (V)_3	600	0	1.6401	0.00111	0.0273	1.5200	1.6500
CCD Voltage Output Value (V)_4	600	0	0.59354	0.00133	0.03251	0.54200	0.58300
CCD Voltage Output Value (V)_5	600	0	1.7918	0.000735	0.0180	1.7500	1.7900
CCD Voltage Output Value (V)_6	600	0	1.4279	0.00141	0.0346	1.1000	1.4000
CCD Voltage Output Value (V)_7	600	0	1.1837	0.00147	0.0359	0.9170	1.1700
CCD Voltage Output Value (V)_8	600	0	1.0766	0.00168	0.0412	0.9790	1.0600

Figure 4.6: Summary of The CCD Tomography Voltages of Eight Ruby Stone Samples

Table 4.8: Comparison Between the Experimental CCD Tomography Mean Voltages

Experiment number	Mean voltage value (V)
1	1.5104
2	0.5935
3	1.6401
4	0.5935
5	1.7915
6	1.4275
7	1.1837
8	1.0766

The experimental voltages varied due to unstable conditions surrounding the experiments, such as the light intensity of the laser as well as the room and the noise feature of the CCD, which could become saturated when exposed to light over a prolonged period of time (Jamaludin, 2016). The experimental and theoretical values were further analyzed to obtain reliable data and compare the model and actual values to quantitatively grade ruby stones.

4.4.2 Analysis of the Theoretical and Experimental CCD Values

4.4.2.1 Mean Voltages

Table 4.9 compares the experimental and theoretical mean voltages while Table 4.10 compares the number of pixels to validate the ability of CCD tomography to quantitatively grade ruby stones.

Table 4.9: Comparison of Experimental and Theoretical Mean Voltages

Experiment Number	Mean Voltage Value	Difference Between Mean (2.000)	Difference Between Mean (1.994)
1	1.5104	0.4896	0.4836
2	0.5935	1.4065	1.4005
3	1.6401	0.3599	0.3539
4	0.5935	1.4065	1.4005
5	**1.7915**	**0.2085**	**0.2025**
6	1.4275	0.5725	0.5665
7	1.1837	0.8163	0.8103
8	1.0766	0.9234	0.9174

4.4.2.2 Number of Pixels

Table 4.10: Number of Pixels of the Theoretical CCD

Number of experiments	Mean Voltage Value	Number of Pixels (z-axis)
1	1.994	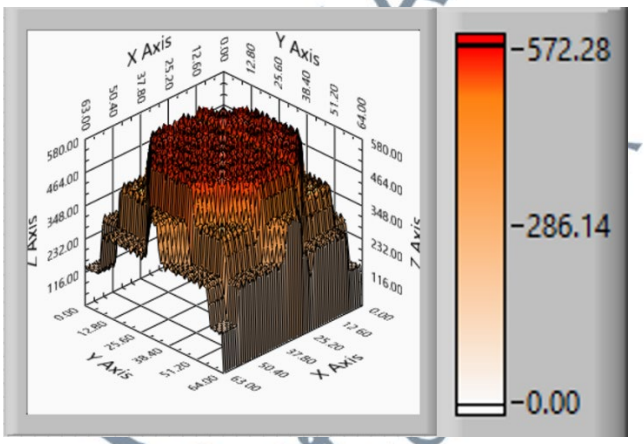 Z axis: 572.28
2	2.000	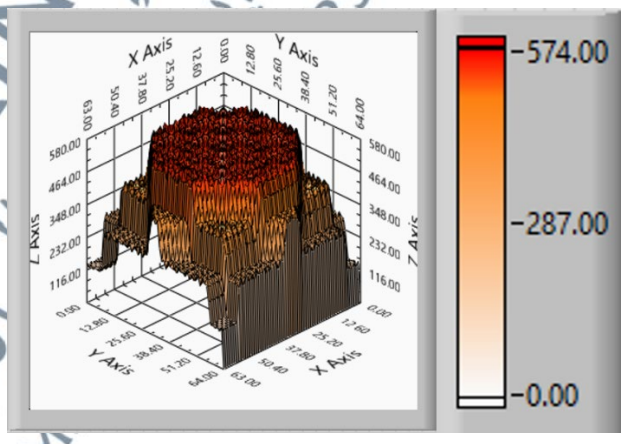 Z axis: 574.00

Table 4.11: Number of Pixels of the Experimental CCD

Number of experiments	Mean Voltage Value	Number of Pixels (z-axis)
1	1.5104	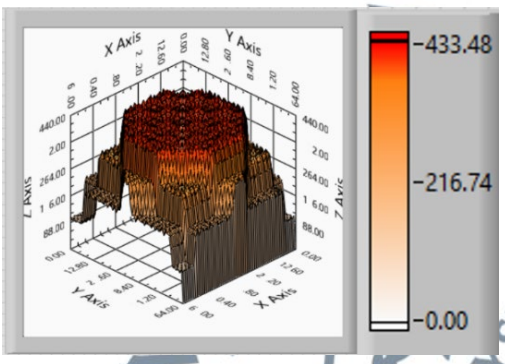 Z-axis: 433.48
2	0.5935	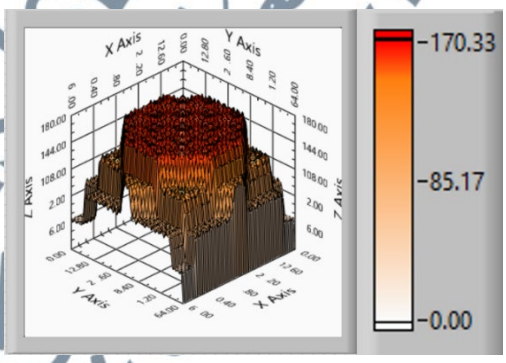 Z-axis: 170.33
3	1.6401	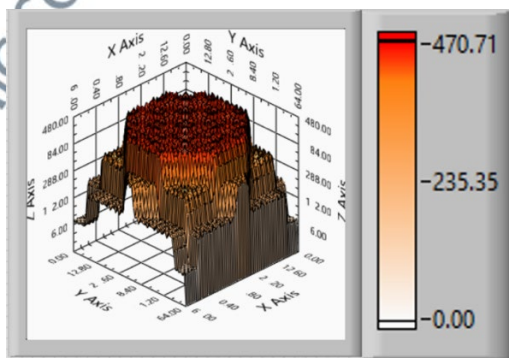 Z-axis: 470.71

Table 4.11: continued

Number of experiments	Mean Voltage Value	Number of Pixels (z-axis)
4	0.5935	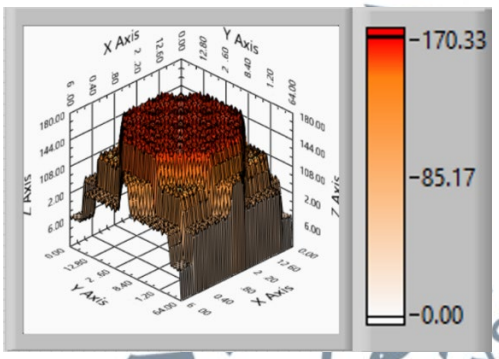 Z axis: 170.33
5	1.7915	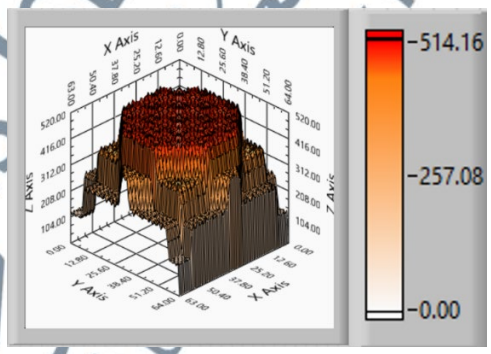 Z axis: 514.16
6	1.4275	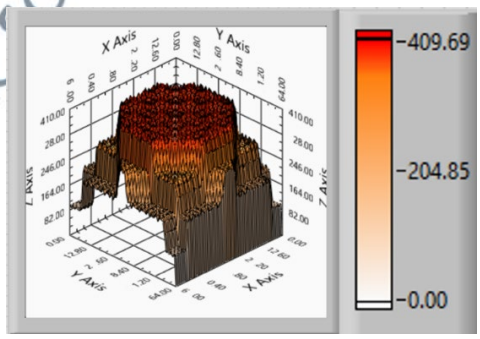 Z axis: 409.69

Table 4.11: continued

Number of experiments	Mean Voltage Value	Number of Pixels (z-axis)
7	1.1837	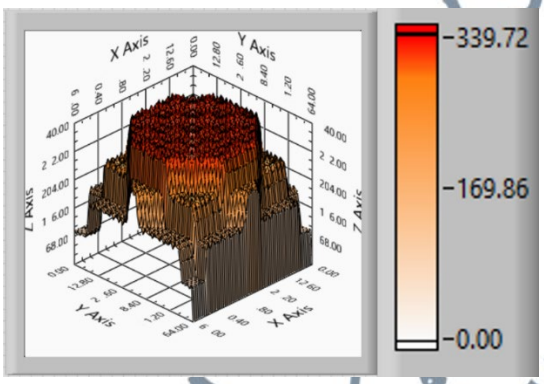 Z-axis: 339.72
8	1.0766	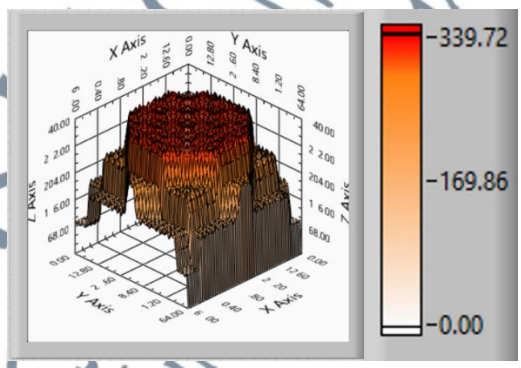 Z-axis: 312.61

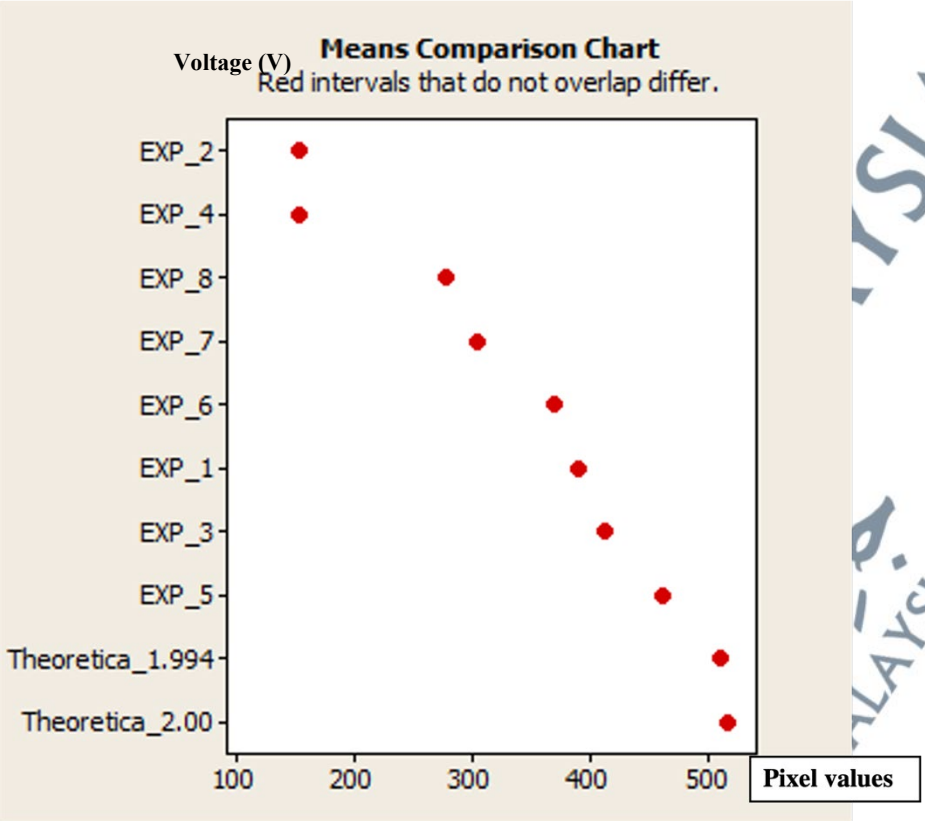

Figure 4.7: Comparison of The Experimental and Theoretical Mean Pixel Values

4.4.2.3 Observations

Tables 4.10 and Table 4.11 as well as Figure 4.7 compared the mean voltages and pixel values. The theoretical voltage (1.994 V) was closest to the experimental voltage (1.7915V) at the fifth experiment. Therefore, these two values were statistically analyzed to validate the CCD tomography system's ability to quantitatively grade ruby stones.

4.4.2.4 Image Reconstruction Analysis

Table 4.12 provides a comparison of the 3D image reconstructions of the theoretical and experimental values. The Z-axis of the theoretical model exhibited a

higher voltage, 1.994 V, resulting in a higher pixel value, 572.28. Meanwhile, the experimental model exhibited a voltage of 1.7915 V and produced only 514.16 pixels, which was lower than the theoretical model.

Table 4.12: 3D Image Reconstructions Using Theoretical and Experimental Values

Output	**Theoretical Value**	**Experimental Value**
Voltage Value (V)	1.994	1.7915
Three-Dimensional form	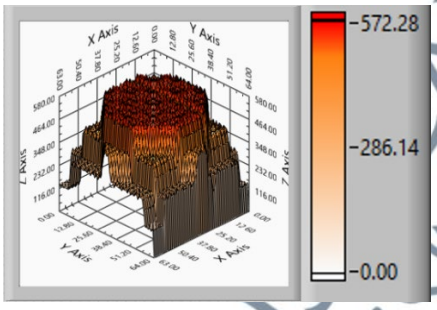 Z-axis ≥ 572.28	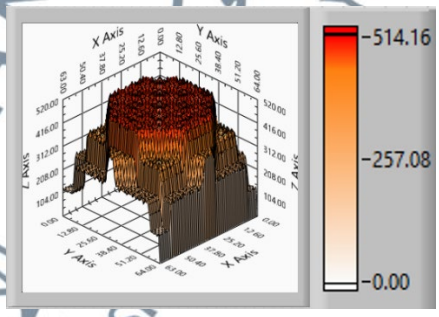 Z-axis ≤ 514.16

4.4.2.5 Statistical Analysis

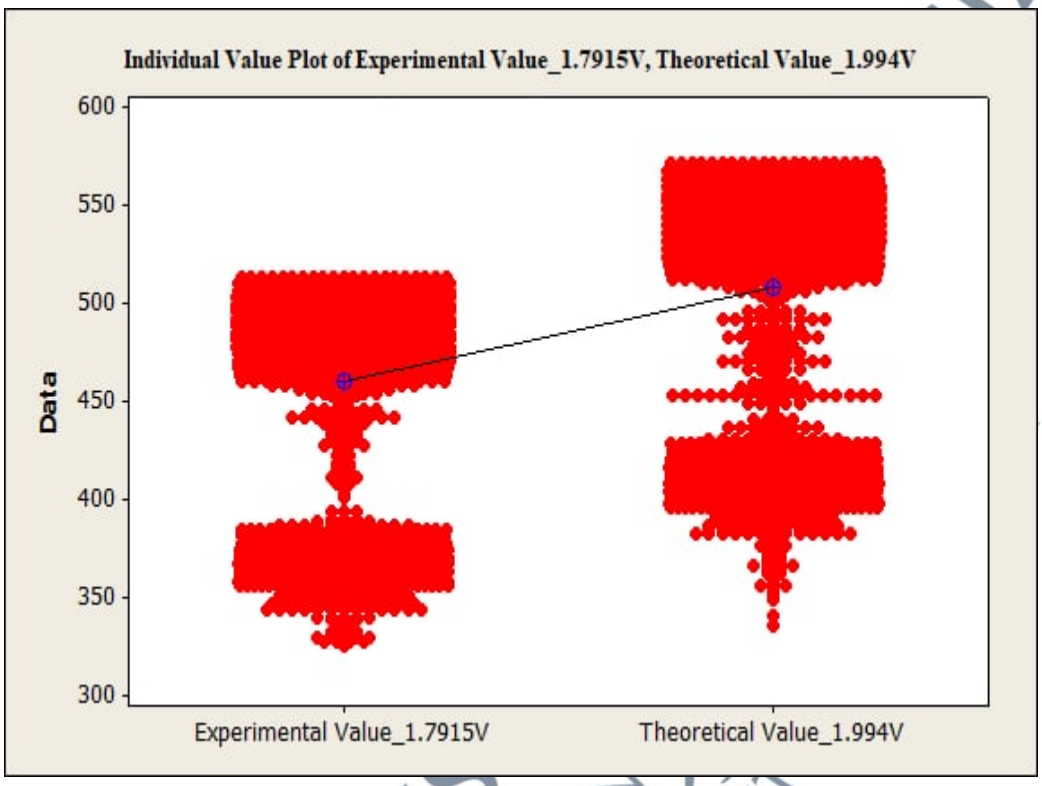

Figure 4.8: Individual Plot of Experimental and Theoretical Mean Pixel Values

```
Level                          N    Mean  StDev
Experimental Value_1.791    2647  460.53  52.23
Theoretical Value_1.994V    2647  509.09  58.89

                           Individual 95% CIs For Mean Based on
                           Pooled StDev
Level                      ----+---------+---------+---------+-----
Experimental Value_1.791   (*)
Theoretical Value_1.994V                                    (*-)
                           ----+---------+---------+---------+-----
                             465       480       495       510
```

Figure 4.9: Summary of Experimental and Theoretical Values

Theoretical value was the value expected from the equation of the light optical properties of the ruby stone while the experimental value was what was actually measured during the experiment. As seen in Figure 4.7 and Figure 4.8, there was a slight difference in the mean experimental and theoretical pixel values; 1.7915 and 1.994, respectively. The following relative error formula was used to calculate the difference between the mean experimental and theoretical voltages of ruby stones:

$$\frac{Experimental\ Value - Theoretical\ Value}{Theoretical\ Value}\ x\ 100 \quad (4.1)$$

Based on these equations, the error of the experimental and theoretical values was −0.1015 or −10.15%. This is an acceptable range for a statistical analysis formula (Zhang et al., 2007). Therefore, this value validated the CCD tomography system's ability to grade ruby stones quantitatively.

4.5 Results Discussion

The present study results validate the ability of the CCD tomography system with a laser as a transmitter to distinguish between different grades of ruby stone clarity. It was also consistent with existing studies that found the system can measure and capture varying levels of object transparencies and opacities (Jamaludin, 2016; Jamaludin et al., 2020; Jamaludin, Abdul Rahim, et al., 2016; Jamaludin, Rahim, et al., 2018; Jamaludin, Rahim, Rahim, et al., 2017; Jamaludin & Abdul Rahim, 2016; Mohd Rahalim et al., 2021).

Ruby stones with higher clarity are more expensive than rubies with lower clarity as this indicates the presence of inclusion, or unwanted materials, in the stones

(Renfro et al., 2018; Walter, 2021). According to Gems and Gemstone: Timeless Natural Beauty of the Mineral World by Grande & Augustyn (2010), ruby stones are of excellent quality, and higher-priced, when the clarity has very slight inclusion. Table 2.1 in Chapter 2 provides a summary of ruby stone prices.

The present study's findings indicate that ruby stones with lower refractive indices have higher clarity. This causes the CCD to exhibit a voltage output that is higher and proportional to the Z-axis value of the 3D images in LabVIEW. Therefore, this present study could successfully grade ruby stones quantitatively using clarity